Toxicology Reports 1 (2014) 114–121

Contents lists available at ScienceDirect

Toxicology Reports

journal homepage: www.elsevier.com/locate/toxrep

Nickel nanowires induce cell cycle arrest and apoptosis by generation of reactive oxygen species in HeLa cells

ChangGuo Ma[a], MengMeng Song[b,c], Ye Zhang[b], ManQing Yan[b], Min Zhang[a,*], Hong Bi[b,**]

[a] School of Life Sciences, Anhui University, Hefei 230601, PR China
[b] College of Chemistry and Chemical Engineering, Anhui University, Hefei 230601, PR China
[c] School of Medical Science, Anhui Medical University, Hefei 230032, PR China

ARTICLE INFO

Article history:
Received 29 January 2014
Received in revised form 28 April 2014
Accepted 28 April 2014
Available online 16 May 2014

Chemical compounds studied in this article:
Thiazolyl blue (PubChem CID: 64965)
Sodium dodecyl sulfate (PubChem CID: 3423265)
Dimethylformamide (PubChem CID: 6228)
DAPI (PubChem CID: 2954)
Propidium iodide (PubChem CID: 104981)
2′,7′-Dichlorodihydrofluorescein diacetate (PubChem CID: 77718)
5,5′,6,6′-Tetrachloro-1,1′ 3,3′tetraethyl-imidacarbocyanine iodide (PubChem CID: 5353694)

Keywords:
Ni NWs
ROS
Apoptosis
Cell cycle arrest
Cytotoxicity

ABSTRACT

Nickel nanowires (Ni NWs) have great potential to be used as a living cell manipulation tool and developed into an anticancer agent. However, their candidacy as biomedical appliances need detailed human cell studies, such as study of the interaction between Ni NWs and tumor cells. The present study investigated the cytotoxicity of Ni NWs in HeLa cells. A dose-dependent inhibition of cell growth was observed by using the MTT assay. We demonstrated that Ni NWs induced oxidative stress by generation of reactive oxygen species (ROS). Apoptosis induction was evidenced by flow cytometry, annexin V binding assay and DAPI staining. DNA flow cytometric analysis indicated that Ni NWs significantly increased the percentages of cells in S phase compared with control cells. This process was accompanied by the loss of mitochondrial membrane potential. These results revealed that Ni NWs induced apoptosis in HeLa cells via ROS generation and cell cycle arrest.
© 2014 The Authors. Published by Elsevier Ireland Ltd. This is an open access article under the CC BY-NC-ND license (http://creativecommons.org/licenses/by-nc-nd/3.0/).

1. Introduction

One-dimension magnetic metallic nanowires have received considerable attention in nanobiomedicine given its outperformance in nanobiotechnology [1–4]. Among a variety of nanowires, nickel nanowires (Ni NWs) have shown advantages for bio-application. Ni NWs have great potential to become a living cell manipulation tool because it can be easily internalized by cells and used to separate

* Corresponding author. Tel.: +86 18019931655.
** Corresponding author. Tel.: +86 15855175680.
E-mail addresses: zhmin07@ustc.edu.cn (M. Zhang), bihong@ahu.edu.cn (H. Bi).

http://dx.doi.org/10.1016/j.toxrep.2014.04.008
2214-7500/© 2014 The Authors. Published by Elsevier Ireland Ltd. This is an open access article under the CC BY-NC-ND license (http://creativecommons.org/licenses/by-nc-nd/3.0/).

cells [5–7]. In addition, Ni NWs could be an anticancer agent that induces tumor cell death [8]. However, the effects of Ni NWs on tumor cells and possible health risks have not been fully evaluated.

Oxidative stress mediated by reactive oxygen species (ROS) is a key mechanism for the cytotoxicity of nanomaterials [9,10] and is one of the essential mechanisms that cause cell apoptosis. Excessive ROS can induce DNA damage, which results in cell cycle arrest for DNA repair [11,12]. If the DNA damage cannot be repaired, the cell is eliminated through apoptosis [13,14]. ROS can also induce disruption of the mitochondrial membrane potential (MMP) and release of cytochrome c from mitochondria into the cytoplasm, where cytochrome c initiates a caspase cascade that terminates cell by causing apoptosis [15,16].

Ni NWs are fiber-shaped nanomaterials. The length of fiber was deemed to be a critical factor in determining cytotoxicity of the fiber. The cytotoxicity of many fibrous materials has been reviewed in detail [17]. In general, long fiber was more toxic than short ones. Previous study reported that the cytotoxicity of long Ni NWs (~20 μm) was significant in THP-1 cells [18]. For biomedical application, the length of NWs should be short, and, therefore, the short Ni NWs (~1 μm) were prepared and their cytotoxicity was evaluated in the present study. We chose HeLa cells, one of the most commonly used tumor cells, as a model to investigate the cytotoxicity of Ni NWs. The cytotoxicity of the short Ni NWs was indeed lower than that reported for the longer ones (20 μm). However, with the increased concentration of short Ni NWs, cytotoxicity was also detected. We showed that the short Ni NWs can induce oxidative stress, cell cycle arrest, mitochondrial depolarization and cell apoptosis in HeLa cells. These results suggested that making Ni NWs short can reduce cytotoxicity, but short Ni NWs also exhibit cytotoxicity in a dose-dependent manner. This work may have important implications when considering the hazard posed by Ni NWs and their regulation for bio-application. This preliminary study also provides insight into the apoptotic cell death induced by Ni NWs in HeLa cells and suggests possible cellular mechanisms involved for the ROS-mediated oxidative stress.

2. Materials and methods

2.1. Preparation and characterization of Ni NWs

Ni NWs were prepared by electrodeposition in the nanopores of the anodic aluminum oxide (AAO) templates. The AAO templates were prepared by means of one-step electrochemical anodization followed by a voltage decreasing process [3]. Briefly, the 99.999% aluminum foil was anodized in 0.4 M $H_2C_2O_4$ aqueous solution under a constant voltage of 40 V for 5 h at 0 °C. Subsequently the voltage was reduced from 40 V to 10 V at a rate of 1.0 V/min in order to make the oxide barrier layer thinner at the bottom. The Ni NWs electrodeposition was performed in 120 g/L $NiSO_4{\cdot}7H_2O$, 45 g/L H_3BO_3, and 17 g/L $(NH_4)_2SO_4$, using an applied alternative current voltage of 10 V. After deposition, the remaining aluminum was removed by a $HgCl_2$ aqueous solution. The template was dissolved in 1 M NaOH aqueous solution, and the NWs were suspended in the solution. Once in suspension, the wires were collected with a magnet and washed with redistilled water until the pH was neutral.

The morphology of Ni NWs was observed by scanning electron microscope (SEM, JEM-2100, JEOL Ltd. Japan). Elemental composition of Ni NWs was analyzed by energy dispersive spectrometers (EDS). Samples for EDS were mounted on a carbon-coated-copper grid.

2.2. Cell culture and treatment of Ni NWs

HeLa cells were obtained from the American Type Culture Collection (ATCC) (Manassas, VA). HeLa cells were cultured in DMEM (Hyclone, USA) medium supplemented with 10% fetal calf serum (Hyclone, USA) and 1% penicillin and streptomycin (Hyclone) at 37 °C. These cells were placed under a humidified atmosphere of 5% CO_2. For all experiments, cells were seeded to provide experimental stage 80% confluence in 6-, 24-, or 96-well plates and grown for 24 h. The Ni NWs were diluted in DMEM medium and mixed thoroughly. The concentration of Ni NWs was defined as the number ratio of Ni NWs to cell instead of the common mass concentration. To calculate the total number of Ni NWs, the mass was divided by the average mass of a single NW. The mass of a single wire was determined by the density of Ni (8.90 g/cm^3) multiplied by the average volume of a single Ni NW. Upon reaching 80% adherent confluence, cells were treated with appropriate concentrations of Ni NWs suspended in cell culture medium with 10% serum for the desired time.

2.3. MTT assay

MTT [3-(4,5-dimethylthiazol-2-yl)-2,5-diphenyltetrazolium bromide] assay was performed to evaluate cell growth inhibition. Cells were treated with Ni NWs at various concentrations for 24 h. After 24 h of incubation, suspension medium was replaced and 25 μl MTT (5 mg/ml in PBS solution) was added into each well. After 2 h of incubation, culture supernatants were aspirated, and purple insoluble MTT product was re-dissolved in 100 μl SDS-DMF (20% SDS mixed in 50% DMF) for an additional 6 h incubation. The concentration of the reduced MTT in each well was measured at 570 nm using a micro-plate reader. Cell viabilities were presented as the percentage of the absorbance of Ni NWs-treated cells to the absorbance of non-treated cells and plotted against Ni NWs concentration.

2.4. DAPI staining

HeLa Cells were treated with Ni NWs at the concentration of 10,000 NWs per cell for 24 h. 50 μg/mL DAPI (Beyotime, Shanghai, China), a DNA-specific fluorescent dye, was added to each well and incubated for 15 min at 37 °C. The stained cells were visualized under a fluorescent microscope (Olympus IX51, Tokyo, Japan).

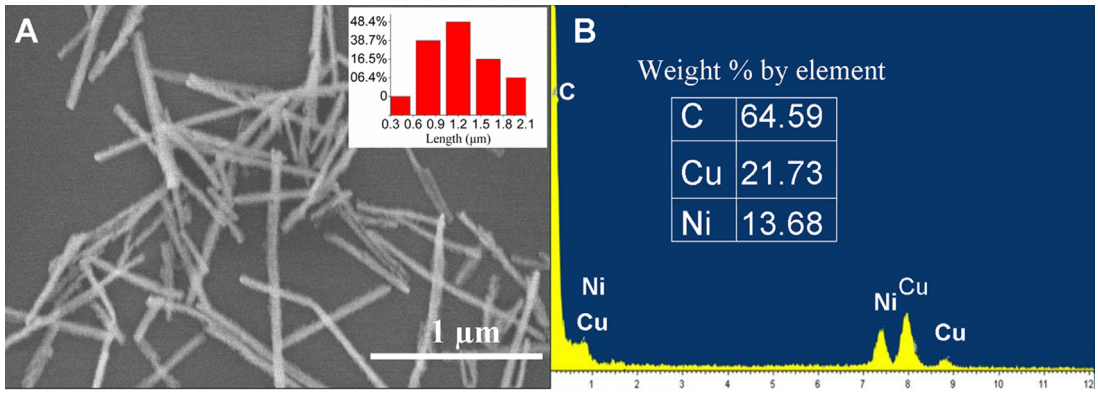

Fig. 1. Characterization of Ni NWs. (A) SEM image of Ni NWs, with inset showing the percentages of Ni NWs of different lengths. (B) Energy dispersive spectrum of Ni NWs for elemental analysis.

2.5. Apoptosis assay

Apoptosis in HeLa cells was measured by the Annexin V/Propidium Iodide (PI) Apoptosis Detection Kit (Beyotime). Briefly, HeLa cells were exposed to different concentrations of Ni NWs in 6-well plates for 24 h. After exposure, cells were trypsinized and centrifuged at 1000 rpm. The cell pellet was washed with PBS once and re-suspended in 100 μL binding buffer, then incubated with 2 μL annexin V-FITC for 10 min, which was followed by staining with 2 μL PI. Then, the samples were diluted with 400 μL binding buffer and analyzed with a flow cytometer (Becton Dickinson, Franklin Lakes, NJ, USA). The different labeling patterns in the annexin V/PI analysis were used to identify the different cell populations where FITC-negative and PI-negative cells were designated as viable cells. FITC-positive and PI-negative cells were identified as early-apoptotic cells. FITC-positive and PI-positive cells were identified as late-apoptotic cells. FITC-negative and PI-positive cells were identified as necrotic cells. The data analysis was performed using BD FACS Diva software (Becton Dickinson).

2.6. Detection of ROS

The intracellular ROS level was detected by DCFH-DA (2′,7′-dichlorodihydrofluorescein diacetate) staining. DCFH-DA can enter into cells as a fluorescent probe and be deacetylated to form DCFH trapped in cells. DCFH is non-fluorescent unless oxidized by intracellular ROS to transform DCF. The fluorescence intensity of DCF can indicate intracellular ROS level. HeLa cells were first exposed to Ni NWs at different concentrations for 24 h. For fluorescence microscope imaging, the cells were washed three times with PBS and incubated with 10 μmol/L DCFH-DA (Beyotime) for 20 min. After washing with DMEM twice, the cells were observed with a fluorescence microscope (Olympus IX51). For fluorometric analysis, cells were trypsinized and washed three times with PBS, then incubated with 10 μmol/L DCFH-DA for 20 min. After washing twice with DMEM, the cells were analyzed by flow cytometry (Becton Dickinson).

2.7. Cell cycle analysis

Cell cycle analysis was carried out according to instructions of the Cell Cycle and Apoptosis Analysis Kit (Beyotime). Briefly, after plating 1×10^6 cells on 6-well plates for 24 h, cells were incubated with various concentrations of Ni NWs for 24 h. Thereafter, cells were trypsinized, washed with PBS and fixed with 75% ethanol overnight at 4 °C. The fixed cells were washed with PBS and incubated with PI and RNase (700 U/ml) for 1 h. Measurement was carried out by using a flow cytometer (Becton Dickinson).

2.8. Detection of mitochondrial membrane potential (MMP) depolarization

MMP was determined using the mitochondrial permeability dye JC-1 (5,5′,6,6′-tetrachloro-1,1′,3,3′-tetraethylimidacarbocyanine iodide). This dye reagent enters the mitochondria, aggregates, and fluoresces red. When the mitochondrial membrane potential collapses, the dye reagent can no longer accumulate within the mitochondria and fluoresces green. HeLa cells were cultured with different concentrations of Ni NWs in 6-well plates for 24 h and were rinsed with PBS twice, and stained with 5 mmol/L JC-1 (Beyotime) for 30 min at 37 °C. Then cells were rinsed twice with ice-cold PBS, re-suspended in 200 μL ice-cold PBS, and instantly assessed for red and green fluorescence with flow cytometry (Becton Dickinson).

2.9. Determination of Ni^{2+} Concentrations in culture medium

For measurement of the Ni^{2+} release in culture medium, the Ni NWs were dispersed directly in DMEM at various concentrations and incubation for 24 h at 37 °C. Ni NWs were separated by centrifugation of NWs suspensions for 30 min at 12,000 × *g*. The supernatant containing the Ni^{2+} from NWs was analyzed by inductively coupled plasma optical emission spectrometry (ICP-OES, Thermo Fisher Scientific, Pittsburgh, PA, USA).

2.10. Statistical analysis

All results were expressed as mean ± SD of three identical experiments, each done in three replicates. Statistical significance was determined by one-way analysis of variance (ANOVA) followed by Dunnett's multiple comparison test. Significance was ascribed at $p < 0.05$.

3. Results

3.1. Characterization of Ni NWs

Electrochemical deposition has been widely used to prepare metal NWs. Here Ni NWs were prepared by electrodeposition in the nanopores of AAO template. SEM was used to observe the morphology of Ni NWs liberated from the AAO template (Fig. 1A). The diameter of the fabricated Ni NWs was about 50 nm, and the average length of the Ni NWs was about 1 μm.

The energy dispersive spectrum demonstrated the presence of Ni, C and Cu (Fig. 1B). The percentages of elemental weights of Ni, C, and Cu were 13.63, 64.59, and 21.73, respectively. The presence of Cu and C signal was from the carbon-coated-copper grid. Therefore, the element composition analysis indicated that the Ni NWs were pure Ni metal.

3.2. MTT assay

MTT assay was used to evaluate the relative cell proliferation (%) of HeLa cells treated with various concentrations of Ni NWs for 24 h. Ni NWs inhibited the growth of HeLa cells in a dose-dependent manner (Fig. 2A). When the number ratio of Ni NWs to cells was 1000:1, the cell viability was about 90%. When the number ratio of Ni NWs to cells increased to 10,000:1, cell viability decreased to about 60%.

3.3. Cell apoptosis induced by Ni NWs

HeLa cells were exposed to Ni NWs of increasing concentrations for 24 h, and cell apoptosis was analyzed by annexin V/PI staining. A proportion of annexin V-stained cells to the total Ni NWs-treated cells increased in a dose-dependent manner (Fig. 2B and C). We also examined the nuclear morphologies of cells using the fluorescent DNA-binding agent DAPI. Dying cells displayed typical morphological features of apoptosis cells (Fig. 2D) at the concentration of 10,000 NWs per cell, while control cells contains normal nucleus. The nucleus gradually became condensed and formed apoptotic bodies in Ni NWs-treated HeLa cells.

3.4. Intracellular ROS generation

After HeLa cells were treated with various concentrations of Ni NWs for 24 h, intracellular ROS generation was determined by the fluorescent probe DCFH-DA. Both fluorescence microscopy (Fig. 3A) and flow cytometry (Fig. 3B) indicated that the green fluorescence intensity of DCF was enhanced in the Ni NWs-treated cells compared with the control cells. These results indicated that Ni NWs induced intracellular ROS generation in a dose-dependent manner.

3.5. Cell cycle arrest assay

PI staining and flow cytometric analysis were used to determine cell cycle distribution in the Ni NWs-treated HeLa cells. Incubation of Ni NWs at various concentrations with HeLa cells for 24 h increased the percentages of sub-G1 and S phase cells compared with the control cells (Fig. 4A and C). A statistically significant difference between the increments of sub-G1 populations among different concentrations of Ni NWs ($p < 0.05$) was observed. These results indicated that Ni NWs induced cell apoptosis and cell cycle arrest at S phase.

3.6. Depolarization of MMP

HeLa cells were treated with different concentrations of Ni NWs for 24 h. After staining with JC-1, the MMP of cells was analyzed by flow cytometry. The percentages of cells with green fluorescence increased and the percentages of cells with red fluorescence decreased in a concentration-dependent manner (Fig. 4B and D), which demonstrated the occurrence of depolarization of MMP.

3.7. Release of Ni^{2+} from NWs in culture medium

The concentrations of Ni^{2+} released from Ni NWs in DMEM were measured. Ni NWs were directly dispersed in DMEM at various concentrations. The dispersions were maintained at 37 °C for 24 h to replicate the conditions in the cell cultures. The concentrations of Ni^{2+} were not significantly different from those in control cultures (Fig. 5). The Ni^{2+} in the control medium was from fetal calf serum. With the concentration of Ni NWs increased, the concentrations of Ni^{2+} slightly increased. This indicated that Ni^{2+} can be released from Ni NWs in the culture medium, but the concentration of Ni^{2+} is very low.

4. Discussion

Previous study indicated that length is a key factor for cytotoxicity of fiber-shaped nanomaterials. The long fiber was more toxic than the short one [17]. In our study, the average length of Ni NWs was about 1 μm (Fig. 1A). The cytotoxicity of long Ni NWs (~20 μm) in THP-1 cells was reported [18]. When the cell viability decreased to about 60% after incubation for 24 h, the number ratio of Ni NWs to cells was 10,000:1 (Fig. 2A) in our study, however the number ratio of long NWs to cell was just 100:1 in their study. This indicated that the cytotoxicity of short Ni NWs in the present study was lower than that of long one. This cytotoxicity difference may be because the length of Ni NWs in our study was very short. These results implied that the cytotoxicity of Ni NWs was also length-dependent. Long Ni NWs was more toxic than the short one. The mechanism of cytotoxicity of long Ni NWs (≥14 μm) may be frustrated phagocytosis [19], but the mechanism of short Ni NWs was not fully clear.

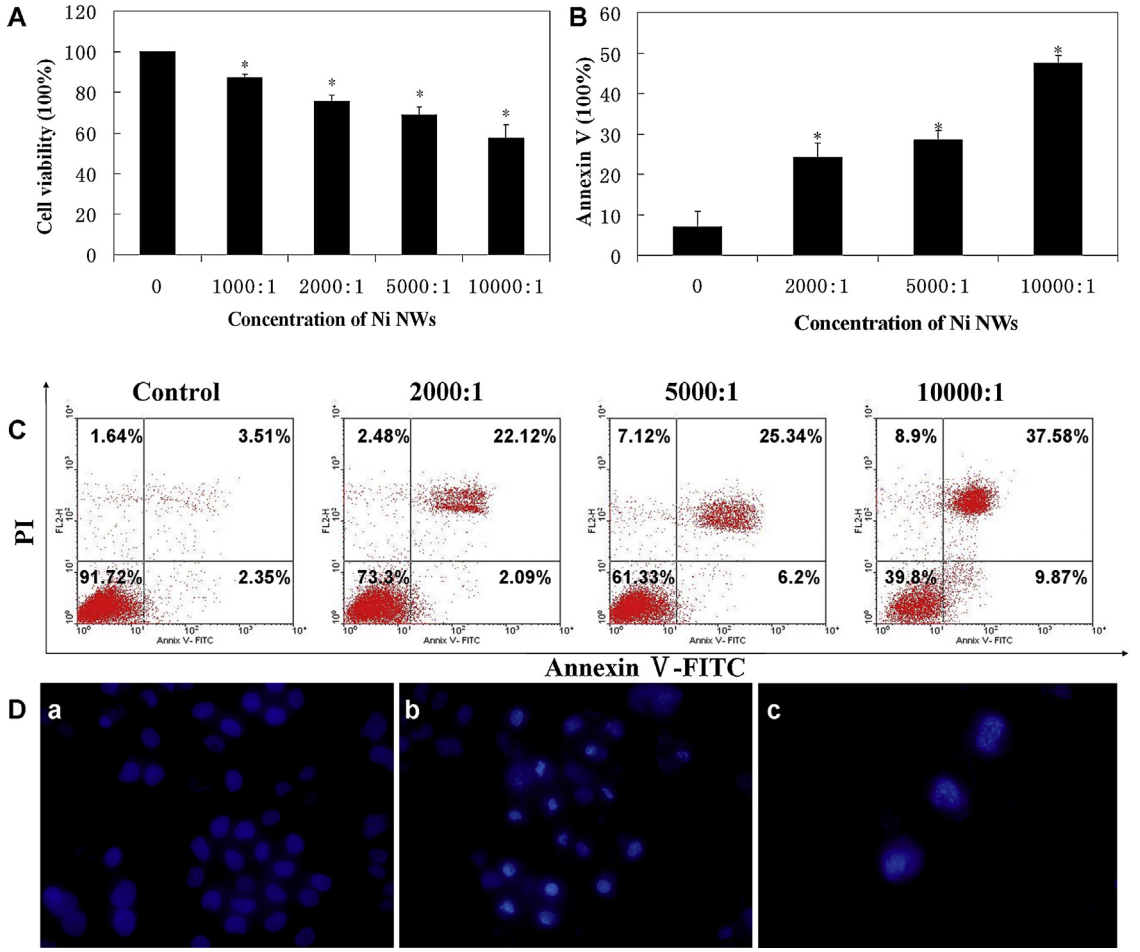

Fig. 2. MTT assay and cell apoptosis induced by Ni NWs in HeLa cells. (A) Cell viability assessed by using the MTT assay. HeLa cells were incubated with various concentrations of Ni NWs for 24 h. Following incubation, viability was assessed using MTT assay. Data are mean ± SD ($n = 3$). Significance was accepted at $p < 0.05$. (B) Bar graph shows the percentages of annexin V positive cells. Data are mean ± SD ($n = 3$). (C) Flow cytometric analysis of HeLa cells after Ni NWs treatment for 24 h. Cells were harvested and stained with annexin V-FITC/PI before analyzed by flow cytometry. (D) Nuclear morphological changes of HeLa cells after treated with Ni NWs at the concentration of 10,000 NWs per cell. After 24 h treatment, cells were stained with DAPI and observed under fluorescence microscope 400×. (a) Control. (b) Chromatin condensation. (c) Apoptotic bodies formation.

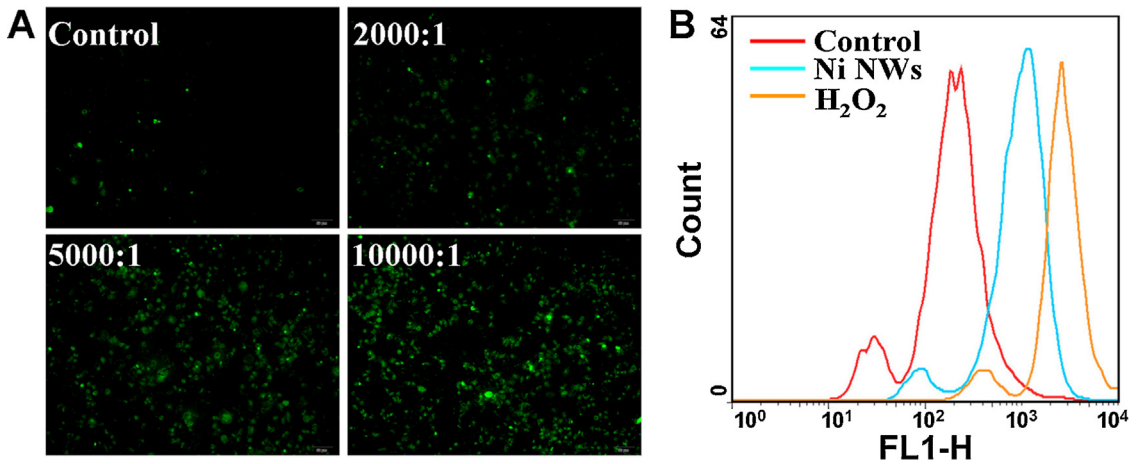

Fig. 3. Intracellular ROS generation in HeLa cells exposed to Ni NWs. (A) Fluorescence microscope (200×) of cells treated with various concentrations of Ni NWs for 24 h. Cells were incubated with DCFH-DA and washed before observation. (B) Fluorescence intensity detected using flow cytometry for HeLa cells treated with Ni NWs at the concentration of 10,000 NWs per cell for 24 h. Cells treated with 0.8 mmol/L H_2O_2 served as positive control.

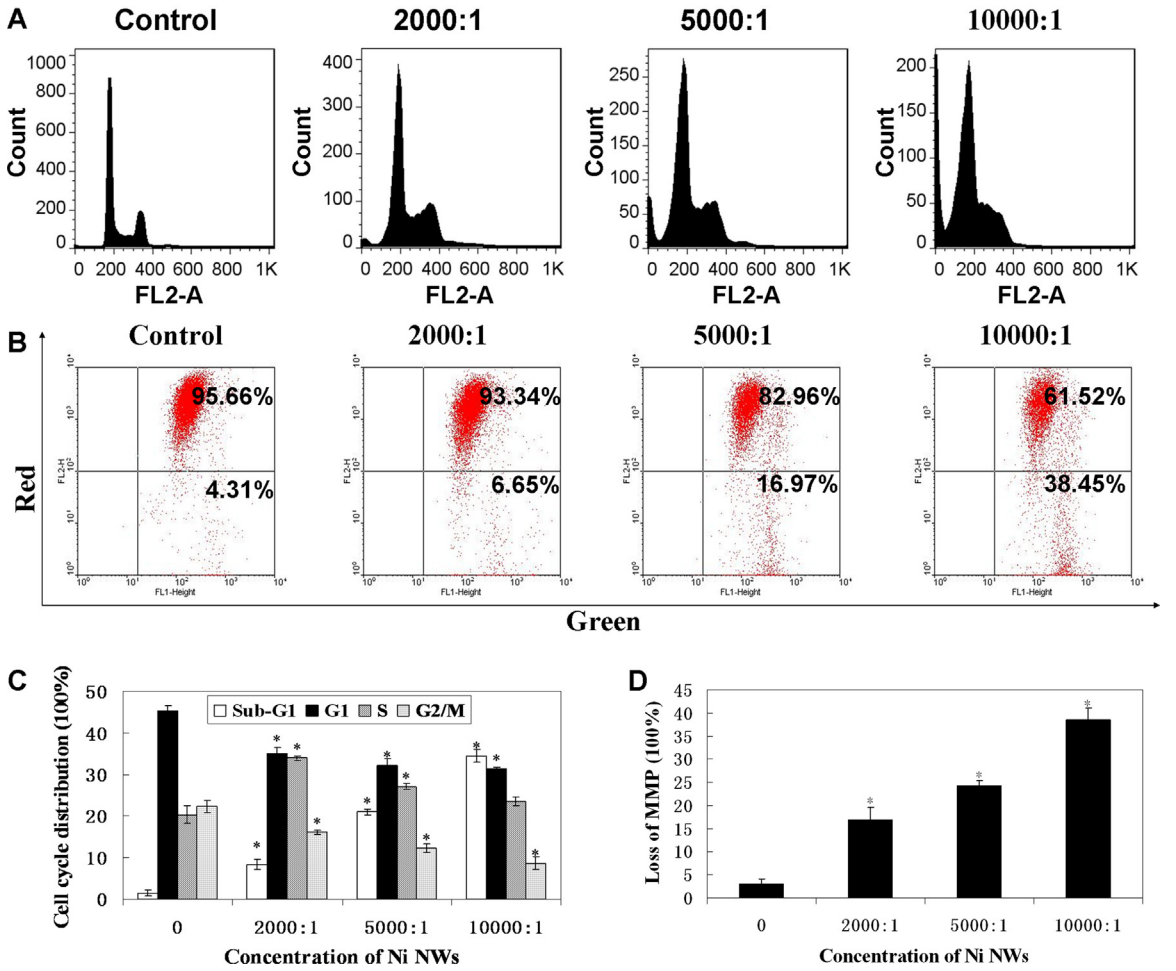

Fig. 4. Cell cycle distribution and MMP changes after incubation with Ni NWs for 24 h. (A) Flow cytometric analysis of cell cycle distribution of HeLa cells. Cells were incubated with various concentrations of Ni NWs for 24 h. (B) Flow cytometry of cells treated with various concentrations of Ni NWs for 24 h, and stained with JC-1. (C) Bar graph of cell cycle distributions. Data are mean ± SD ($n = 3$). (D) Bar graph shows the percentages of cells with MMP decreased. Data are mean ± SD ($n = 3$).

Our study demonstrated that short Ni NWs induced HeLa cell damage via the generation of ROS and the induction of apoptosis. Apoptosis is a normal physiologic process and plays an important role in homeostasis and development of the tissue. During cell apoptotic process, morphological changes including chromatin condensation, DNA fragmentation and apoptotic body formation can be observed [20,21]. To investigate the manner of HeLa cell death, staining with annexin V/PI and DAPI was carried out. The data from the annexin V/PI staining (Fig. 2B and C) indicated that the apoptotic cell populations were increased in a dose-dependent manner. The fluorescent images of cells stained with DAPI (Fig. 2D) indicated that the chromosome condensation and formation of apoptotic bodies in the Ni NWs treated-HeLa cells. These results revealed that apoptosis is a major manner by which Ni NWs induced cell death.

The production of ROS has long been regarded as a mechanism of nanoparticles-induced cytotoxicity [22–24]. The induction of the ROS results in oxidative damage to macromolecules such as proteins, DNA and lipids, finally leads to the damage of different cellular organelles [25,26]. In the present study, ROS significantly increased in the Ni NWs-treated HeLa cells (Fig. 3).

The cytotoxicity of Ni NWs in human pancreatic adenocarcinoma (Panc-1) cells has been reported [8]. Ni NWs induce ROS-mediated apoptosis in Panc-1 cells. In our study Ni NWs can also induce ROS-mediated apoptosis in HeLa cells. These result means that apoptosis is a major mechanism by which Ni NWs induce cell death. When the concentration of Ni NWs was low, cytotoxicity was significant in their study. However, when the concentration of Ni NWs was high, cytotoxicity was greater. This result indicated that the cytotoxicity of Ni NWs in their study was higher than our Ni NWs. This also suggested that the cytotoxicity of Ni NWs was length-dependent because the average length of Ni NWs was 6.5 μm in their study. Both their and our results showed that Ni NWs trigger apoptosis via ROS generation, and we further investigated the function of ROS in apoptosis induced by Ni NWs in HeLa cells.

Oxidative stress is one of several mechanisms that induce cell apoptosis [27,28]. ROS can induce cell apoptosis

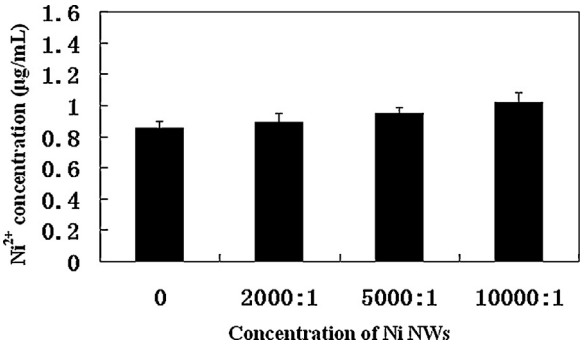

Fig. 5. Ni^{2+} release into cell culture medium. Various concentrations of the Ni NWs were dispersed in DMEM-FBS and incubated for 24 h at 37 °C. The dispersions were then centrifuged at 12,000 × *g* for 30 min, and the Ni^{2+} concentrations in the supernatants were measured by ICP-OES.

through activation of cell cycle checkpoints and mitochondrial apoptotic pathway. Mitochondria are important signaling centers during apoptosis. Cytochrome c exists in the mitochondrial intermembrane space. Cytochrome c release from mitochondria is a core event in the intrinsic apoptotic pathway. When the mitochondrial membrane potential was disrupted, cytochrome c can be released from mitochondria into the cytoplasm. Cytochrome c participates in formation of the apoptosome and caspase-9 activation, and then activates the caspase cascade to induce apoptosis [29]. In our study, Ni NWs induced mitochondrial membrane potential disruption (Fig. 4B and D). There were statistically significant differences among the effects of different concentrations of Ni NWs ($p < 0.05$), which indicated that the mitochondrial membrane potential significantly collapsed. On the one hand, ROS production can directly damage mitochondria. On the other hand, ROS might promote opening of the mitochondrial permeability transition pore through activating cell cycle checkpoints. In the present study, an increase of the percentages of HeLa cells in sub-G1 and S phases (Fig. 4A and C) also shows that cell cycle checkpoints are activated by oxidative stress so that the cell cycle is paused for DNA repair. If the DNA damage cannot be repaired, the ROS might promote opening of the mitochondrial permeability transition pore [30]. Consequently, the outer mitochondrial membrane collapsed, thereby causing the loss of mitochondrial membrane potential. The loss of mitochondrial membrane potential subsequently initiates the release of apoptotic factors, such as cytochrome c, and apoptosis-inducing factors that promote progress of the apoptotic cascade. These results suggested that ROS induce HeLa cell apoptosis through mitochondrial damage or activating cell cycle checkpoints. It also implied that Ni NWs induced cell apoptosis through the mitochondrial pathway.

Ions that are released from the nanoparticles can contribute to their cytotoxicity. The cytotoxicity of Ni^{2+} has been studied. It has been reported that Ni^{2+} can also induce cell apoptosis and DNA damage in T-lymphocyte cells [31]. In addition, Ni^{2+} can result in oxidative stress in cells [32]. In the present study, Ni^{2+} may be released from Ni NWs in the cell and in the cell culture medium (Fig. 5). The ion-releasing properties of the nanoparticles were dependent on the solubility of the nanoparticles. With the same composition, the solubility of small nanoparticles was higher than that of large ones, so the release of ions should be larger for small nanoparticles [33]. The release of Ni^{2+} ions from short Ni NWs should be larger than from long ones. These results mean that the cytotoxicity of short Ni NWs should greater than that of long ones. However the long Ni NWs were more toxic than the short ones. This suggested that the concentration of Ni^{2+} that was released from Ni NWs in the cell or in the cell culture media was very low, and it was insufficient to produce significant cytotoxicity.

In conclusion, our study suggested that the cytotoxicity of Ni NWs was length-dependent. Long Ni NWs were more toxic than short ones. The cytotoxicity of short Ni NWs in HeLa cells was dose-dependent. Ni NWs exhibit multiple anti-proliferative effects, including cell growth inhibition, ROS generation, cell cycle arrest, and cell apoptosis. Overall, our data demonstrated that Ni NWs induce apoptosis in HeLa cells through ROS generation and suggested that ROS induce HeLa cell apoptosis through mitochondrial damage or activation of cell cycle checkpoints. Further studies are needed to investigate the role of ROS in signaling pathways of apoptosis in response to exposure to Ni NWs. This work warrants careful assessment of Ni NWs before their application.

Conflicts of interest

The authors declare they have no conflicts of interest.

Transparency document

The Transparency document associated with this article can be found in the online version.

Acknowledgements

This work was financed by the 211 Project of Anhui University, the National Natural Science Foundations of China (Grant Nos. 20401001, 50772001 and 51272002), Anhui Provincial Natural Science Foundation (1208085ME87), and the Technology Foundation for Selected Overseas Chinese Scholar, Ministry of Personnel of China (No. [2013]-385). This work was also supported by the National Natural Science Foundation of China (Grant No. 51302004) and Anhui Provincial Natural Science Foundation of China (Grant No. 1308085QH141).We also thank the Key Laboratory of Environment-Friendly Polymer Materials of Anhui Province, Anhui University.

References

[1] W. Hallstrom, M. Lexholm, D.B. Suyatin, G. Hammarin, D. Hessman, L. Samuelson, L. Montelius, M. Kanje, C.N. Prinz, Fifteen-Piconewton force detection from neural growth cones using nanowire arrays, Nano Lett. 10 (2010) 782–787.
[2] F. Johansson, M. Jonsson, K. Alm, M. Kanje, Cell guidance by magnetic nanowires, Exp. Cell Res. 316 (2010) 688–694.
[3] M.M. Song, W.J. Song, H. Bi, J. Wang, W.L. Wu, J. Sun, M. Yu, Cytotoxicity and cellular uptake of iron nanowires, Biomaterials 31 (2010) 1509–1517.

[4] M. Tanase, E.J. Felton, D.S. Gray, A. Hultgren, C.S. Chen, D.H. Reich, Assembly of multicellular constructs and microarrays of cells using magnetic nanowires, Lap Chip 5 (2005) 598–605.
[5] N. Gao, H.J. Wang, E.H. Yang, An experimental study on ferromagnetic nickel nanowires functionalized with antibodies for cell separation, Nanotechnology 21 (2010) 105–112.
[6] A. Hultgren, M. Tanase, E.J. Felton, K. Bhadriraju, A.K. Salem, C.S. Chen, D.H. Reich, Optimization of yield in magnetic cell separations using nickel nanowires of different lengths, Biotechnol. Prog. 21 (2005) 509–515.
[7] A. Prina-Mello, Z. Diao, J. Coey, Internalization of ferromagnetic nanowires by different living cells, J. Cardiovasc. Pharmacol. 4 (2006) 9.
[8] M.Z. Hossain, M.G. Kleve, Nickel nanowires induced and reactive oxygen species mediated apoptosis in human pancreatic adenocarcinoma cells, Int. J. Nanomed. 6 (2011) 1475–1485.
[9] H. Meng, T. Xia, S. George, A.E. Nel, A predictive toxicological paradigm for the safety assessment of nanomaterials, ACS Nano 3 (2009) 1620–1627.
[10] A. Nel, T. Xia, L. Madler, N. Li, Toxic potential of materials at the nanolevel, Science 311 (2006) 622–627.
[11] W.P. Roos, B. Kaina, DNA damage-induced cell death by apoptosis, Trends Mol. Med. 12 (2006) 440–450.
[12] M. Valko, M. Izakovic, M. Mazur, C.J. Rhodes, J. Telser, Role of oxygen radicals in DNA damage and cancer incidence, Mol. Cell Biochem. 266 (2004) 37–56.
[13] A.S. Coutts, N. La Thangue, The p53 response during DNA damage: impact of transcriptional cofactors, Transcription 73 (2006) 181–189.
[14] R. Lüpertz, W. Wätjen, R. Kahl, Y. Chovolou, Dose- and time-dependent effects of doxorubicin on cytotoxicity, cell cycle and apoptotic cell death in human colon cancer cells, Toxicology 271 (2010) 115–121.
[15] M.J. Piao, K.A. Kang, I.K. Lee, H.S. Kim, S. Kim, J.Y. Choi, J. Choi, J.W. Hyun, Silver nanoparticles induce oxidative cell damage in human liver cells through inhibition of reduced glutathione and induction of mitochondria-involved apoptosis, Toxicol. Lett. 201 (2011) 92–100.
[16] L. Sun, Y. Li, X. Liu, M. Jin, L. Zhang, Z. Du, C. Guo, P. Huang, Z. Sun, Cytotoxicity and mitochondrial damage caused by silica nanoparticles, Toxicol. In Vitro 25 (2011) 1619–1629.
[17] K. Donaldson, F. Murphy, A. Schinwald, C.A. Rodger DuffPoland, Identifying the pulmonary hazard of high aspect ratio nanoparticles to enable their safety-by-design, Kidney Int. Suppl. 6 (2011) 143–156.
[18] F. Byrne, A. Prina-Mello, A. Whelan, B.M. Mohamed, A. Davies, Y.K. Gun'ko, J.M.D. Coey, Y. Volkov, High content analysis of the biocompatibility of nickel nanowires, J. Magn. Magn. Mater. 321 (2009) 1341–1345.
[19] A. Schinwald, K. Donaldson, Use of back-scatter electron signals to visualise cell/nanowires interactions in vitro and in vivo; frustrated phagocytosis of long fibres in macrophages and compartmentalisation in mesothelial cells in vivo, Part. Fibre Toxicol. 9 (2012) 34.
[20] H.X. Li, P. Wang, Q.H. Liu, X.X. Cheng, Y.T. Zhou, Y.P. Xiao, Cell cycle arrest and cell apoptosis induced by Equisetum hyemale extract in murine leukemia L1210 cells, J. Ethnopharmacol. 144 (2012) 322–327.
[21] H. Yoshihiro, Chromosomal DNA fragmentation in apoptosis and necrosis induced by oxidative stress, Biochem. Pharmacol. 66 (2003) 1527–1535.
[22] N. Lewinski, V. Colvin, R. Drezek, Cytotoxicity of nanoparticles, Small 4 (2008) 26–49.
[23] N. Singh, B. Manshian, G.J.S. Jenkins, S.M. Griffiths, P.M. Williams, T.G.G. Maffeis, C.J. Wright, S.H. Doak, NanoGenotoxicology: the DNA damaging potential of engineered nanomaterials, Biomaterials 30 (2009) 3891–3914.
[24] D.W. Xiong, T. Fang, L.P. Yu, X.F. Sima, W.T. Zhu, Effects of nano-scale TiO_2, ZnO and their bulk counterparts on zebrafish acute toxicity, oxidative stress and oxidative damage, Sci. Total Environ. 409 (2011) 1444–1452.
[25] M.K. Hailer, P.G. Slade, B.D. Martin, T.A. Rosenquist, K.D. Sugden, Recognition of the oxidized lesions spiroiminodihydantoin and guanidinohydantoin in DNA by the mammalian base excision repair glycosylases NEIL1 and NEIL2, DNA Repair 4 (2005) 41–50.
[26] S.E. Sabatini, A.B. Juarez, M.R. Eppis, L. Bianchi, C.M. Luquet, M.D.R. de Molina, Oxidative stress and antioxidant defenses in two green microalgae exposed to copper, Ecotoxicol. Environ. Safe. 72 (2009) 1200–1206.
[27] A. Maqusood, J.A. Mohd, A.S. Maqsood, Oxidative stress mediated apoptosis induced by nickel ferrite nanoparticles in cultured A549 cells, Toxicology 283 (2011) 101–108.
[28] G. Sumonto Mitra Ruchi, A. Waseem, K.S. Siddiqui, Tributyltin induces oxidative damage, inflammation and apoptosis via disturbance in blood–brain barrier and metal homeostasis in cerebralcortex of rat brain: an in vivo and in vitro study, Toxicology 310 (2013) 39–52.
[29] P. Nigro, E. Bloise, M.C. Turco, A. Skhirtladze, P. Montoro, C. Pizza, S. Piacente, M.A. Belisario, Antiproliferative and pro-apoptotic activity of novel phenolic derivatives of resveratrol, Life Sci. 81 (2007) 873–883.
[30] Y-L. Lo, W. Wang, C-T. Ho, 7,3,4′-Trihydroxyisoflavone modulates multidrug resistance transporters and induces apoptosis via production of reactive oxygen species, Toxicology 302 (2012) 221–232.
[31] A. Au, J. Ha, M. Hernandez, A. Polotsky, D.S. Hungerford, C.G. Frondoza, Nickel and vanadium metal ions induce apoptosis of T-lymphocyte Jurkat cells, Int. J. Mod. Phys. C 79A (2006) 512–521.
[32] H.L. Shi, L.G. Hudson, K.J. Liu, Oxidative stress and apoptosis in metal ion-induced carcinogenesis, Free Radic. Biol. Med. 37 (2004) 582–593.
[33] M. Horie, K. Nishio, K. Fujita, H. Kato, A. Nakamura, S. Kinugasa, Ultrafine NiO particles induce cytotoxicity in vitro by cellular uptake and subsequent Ni(II) release, Chem. Res. Toxicol. 22 (2009) 1415–1426.